Flow Visualization of Shock Wave/Boundary-Layer Interaction Controlled by Micro-Ramp at Mach 5

Mohd Rashdan Saad, Azam Che Idris*, Hossein Zare-Behtash** and Konstantinos Kontis***
**Faculty of Engineering, National Defence University of Malaysia*
Kem Sungai Besi, 57000 Kuala Lumpur Malaysia
***School of Engineering, University of Glasgow*
James Watt South Building, Glasgow G12 8QQ United Kingdom

Abstract

Shock-Boundary Layer Interaction is a phenomenon occurring in high-speed air-breathing propulsion systems that is highly undesirable. Numerous methods have been tested to manipulate and control SBLI which includes both active and passive flow control techniques. To determine the improvements brought by the flow control techniques, advanced and state-of the-art flow diagnostics and experimental techniques are required, especially when it involves high-speed flows. In this study, a number of advanced flow diagnostics were employed to investigate the effect of micro-vortex generators in controlling SBLI in Mach 5 such as Pressure Sensitive Paints (PSP), schlieren photography and oil-flow visualization. The flow diagnostics successfully visualized the boundary layer separation and also the improvements brought by the micro-vortex generators.

1. Introduction

The prominent problem faced by hypersonic aero-vehicles propulsion system is the phenomenon called Shock Wave-Boundary Layer Interaction (SBLI) that causes the boundary layer to separate due to the adverse pressure gradients created when the shock wave impinges on the hypersonic boundary layer. This eventually leads to total pressure loss and flow distortion in the intake section [1,2]. As a result, the overall propulsive efficiency of a hypersonic vehicle will be significantly reduced. Therefore it is essential to employ flow control devices to prevent the boundary layer separation, either at the upstream location of throughout the interaction region itself.

A novel passive flow control device called micro-ramp [3,4], which is one of the micro-vortex generators, has shown great potential in controlling the adverse phenomenon. Micro-ramps have heights smaller than the boundary layer thickness, δ and therefore are submerged inside the boundary layer. The counter-rotating vortices produced by the micro-ramp that travel downstream into the interaction region help to reduce the boundary layer separation by producing upwash and downwash motion which improves the boundary layer state [4].

Due to the nature of experiments that were conducted in high-speed flows, one of the challenges is the selection of the flow diagnostics method. The most commonly used methods are schlieren [3,4], oil-flow visualisation [4,5] and also Particle Image Velocimetry [6]. However majority of the investigations were done in supersonic flow. This paper focuses on the different types of flow diagnostics that were used in the SBLI investigation done in hypersonic flow [7] and how effective are they in revealing useful information on the flow separation control.

2. Experimental Setup

2.1 Hypersonic Wind Tunnel

The experiments were conducted in the Mach 5 High Supersonic Tunnel (HSST) located in the Aero-Physics Laboratory of the School of Mechanical Aerospace and Civil Engineering, University of Manchester. The HSST is a supersonic intermittent blowdown tunnel having the capability of running experiments between Mach 4 to 6 by changing the nozzles. The full schematic diagram of the tunnel is shown in Fig. 1. The unit Reynolds number is 13.2 $\times 10^6$ m^{-1}. The operational stagnation temperature of the wind tunnel was set at 375 K (± 5 K) while the stagnation pressure was 6.50 × 105 Pa (± 5 × 103 Pa). The values of the freestream conditions of the testing are listed in Table 1.

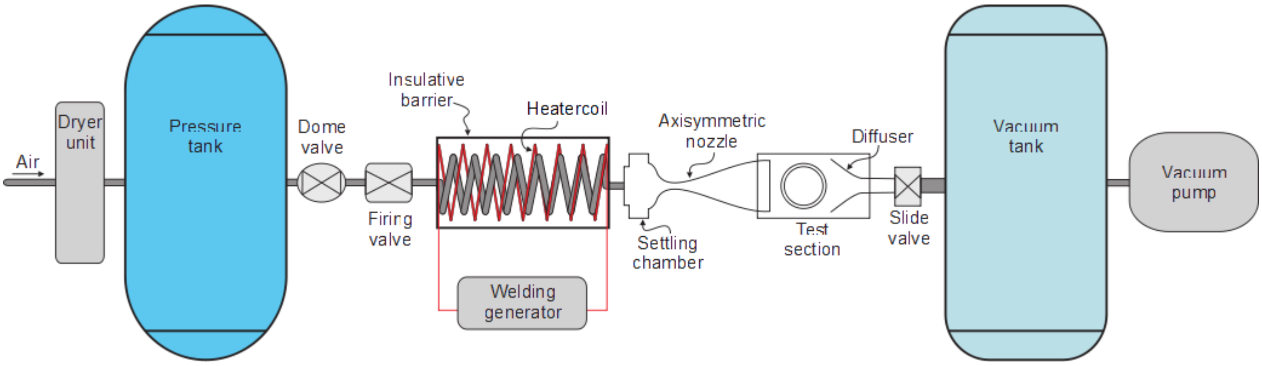

Figure 1: Schematic layout of the Mach 5 HSST wind tunnel at the University of Manchester

Table 1: Freestream values with uncertainties of HSST at Mach 5

Freestream Properties	Value
M	5.0 ± 0.5%
p_0 (mbar)	6450 ± 0.7%
Re ($\times 10^6$)/m	13.1 ± 1.7%
p_{pitot} (mbar)	396 ± 1%
p_∞ (mbar)	12.18 ± 2.4%
u_∞ (m/s)	790 ± 1.0%

2.2 Flat Plate

A thin flat plate made of Aluminium 6082 grade was used throughout this study. The MVG models were fixed to the flat plate by using a number of screws then the flat plate was finally fixed on the floor of the wind tunnel test section by a specially made stand. The length of the plate is 360mm, where a natural turbulent boundary layer flow can be achieved at the location of MVG. Figure 2 shows the dimensions of the flat plate.

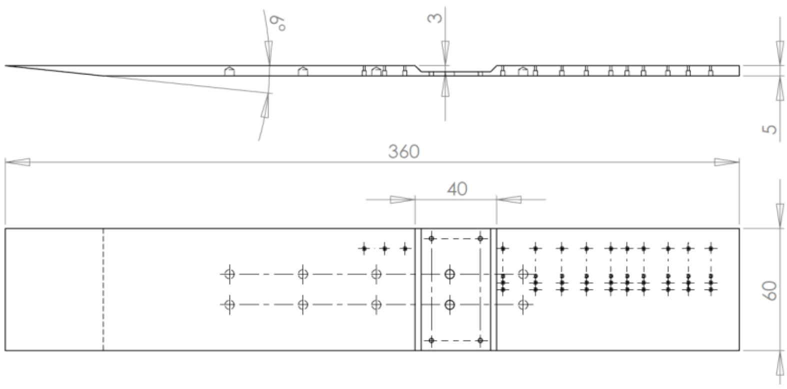

Figure 2: Dimensions of aluminium flat plate

2.3 Shock-Generator

For the purpose of this study, a shock-generator is installed in order to create an oblique shock that impinges on the boundary-layer developed on the flat plate as shown in Figure 3. The shock-generator is installed on the ceiling plate of the test section and creates a 34° oblique shock. X_{SG} and h represents the distance of the leading-edge of the shock-generator in streamwise direction and the vertical distance of the shock-generator from the flat plate, respectively.

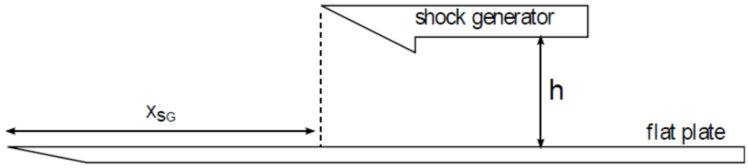

Figure 3: Schematic drawing of the position of the shock-generator with respect to the flat plate

2.4 Micro Vortex Generator (MVG) Model

In this study, two micro-vortex generators were tested. Both of them have the height of 40% and 80% of δ. The value of δ was obtained from preliminary investigation using high-speed schlieren. Both models were sized and designed based on the findings of Anderson et al. [5] where the ratios of dimensions (span, chord length and height) were fixed. The micro-vortex generator were machined on top of a metal strip and attached to the flat plate. The design of the micro-vortex generator is shown in Figure 4.

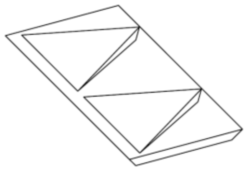

Figure 4: Design of MVG used in this study

2.5 Schlieren Photography Setup

The Toepler's z-type schlieren technique was used in this study which consists of Palflash 501 (Pulse Photonics) continuous light source with a focusing lens and a 2 mm wide slit, two 8 inches parabolic silver coating mirror of 6ft focal length , a knife-edge and a set of Hoya 49mm close-up lens. A Canon digital SLR camera EOS-450D, 12MP and a Photron APX-RS High Speed Video System is being used to capture the images. The complete schematic setup of the schlieren system is shown in Figure 5.

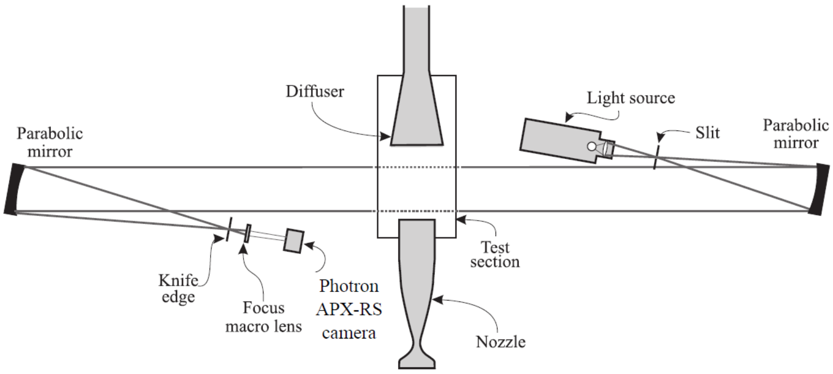

Figure 5: Schematic setup of schlieren photography

2.6 Oil-Flow Visualization

The oil-flow visualization used in this study is intended to reveal the complex flow features on the surface of the model in order to have an initial insight of the flow for subsequent detailed measurements. The viscosity of the oil used plays the most important role. Having a high viscosity will cause the paint a longer time to move and exhibits the desired pattern while having a too runny solution will make the paint to be simply blown away straight after the start of the tunnel. For this facility, it is found that the mixture of paraffin, fluorescent powder, silicon oil and oleic acid satisfies the requirement of the experiment. The fluorescent powder used has the size of $10\mu m$ on average. The setup of the oil-flow visualization consisting of a CCD camera and a set of two UV lights mounted on the wind tunnel is shown in Figure 6.

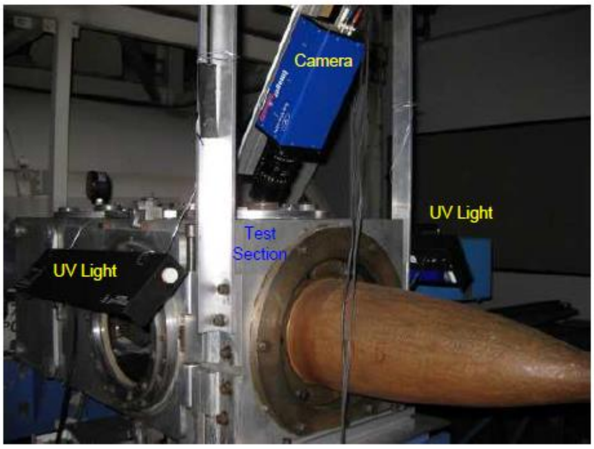

Figure 6: Experimental setup of oil-flow visualization on the wind tunnel

Three different colours were prepared using the same method. By mixing colours, complicated flow features such as separations and flow mixings can be closely captured by the camera. It is also important to ensure that the lighting provided on both sides of the wind tunnel windows have equal illumination intensity to avoid shadows being formed on the surface of the model. A digital SLR camera Nikon D90 12.3 million pixels with 18-105 VR lens was used to record High-Definition videos of the runs.

2.6 Pressure Sensitive Paints (PSP)

The basic operating theory of Pressure Sensitive Paint (PSP) is the illumination of the luminescent molecules that are used as probes at a specific wavelength which results in excitations. The excited molecules then emit lights of longer wavelength that are visible to the image capturing devices. The photons emitted however interact with the oxygen molecules since the polymer binder for the PSP is oxygen permeable. The interaction causes the photons to lose some energy due to the collision with oxygen in a process called oxygen quenching. When the excited luminescent molecules have returned to the ground state while at the same time the emitted photons are being quenched by the oxygen molecules, the luminescence is being decreased as a result. The change in intensity of the surface is recorded by the cameras. The schematic of the working process is illustrated in Figure 7.

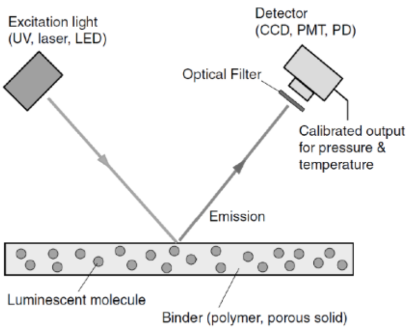

Figure 7: Schematic of a luminescent paint (PSP) system on model surface [8]

During the experiments, the painted models were mounted inside the test section with two UV LEDs panels acting as the excitation light source, shining through the test section window on both sides. Each LED panel consists of 100 blue LEDs arranged in 10×10 array producing the peak wavelength of the emission of 475nm. Both LEDs panels were mounted on the tripods and the tilting angles were adjusted so that the excitation light was equally distributed amongst the entire surface of the model. The signals emitted from the painted model surface were captured by the LaVision Image Intense 12-bit CCD camera that was mounted on top of the test section.

3. Results & Discussions

Figure 8 shows the black and white version of the colour schlieren image. The colour image is being transformed into black and white to reveal more details of the flow. The oblique shock wave created by the shock generator can be clearly seen impinging the incoming turbulent boundary layer creating the separation region. The location of the separation bubble can also be observed in Figure 8 exactly below the location of shock impingement. After the separation region, a series of expansion fans followed by the reattachment shock wave can be visualized. The reattachment shock is the result of the boundary layer reattaching after the separation region where the boundary-layer can be seen to redevelop itself. This proves that from schlieren technique, most of the boundary layer separation features can be detected.

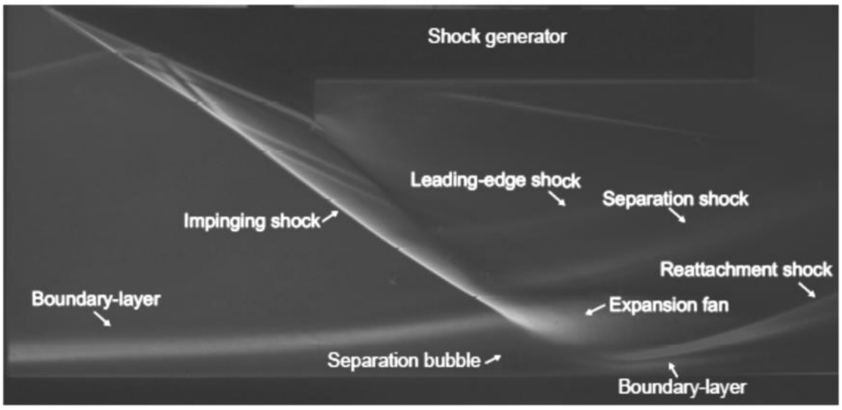

Figure 8: Black and white images of the transformed colour schlieren

Figure 9 shows the high-speed schlieren image of the SBLI condition when flow control is employed using MVG. The turbulent eddies of the incoming boundary-layer are seen in the image and the MVG is submerged in it. The separation bubble still existed even after the flow control. Even though the size of the separation bubble is not clearly visible in the high-speed schlieren images, the separation bubble still exists and this can be deduced from the shocks that appeared in the downstream region. If the separation region is totally eliminated, only one shock can be seen reflecting from the surface of the plate and that will be considered as the shock boundary layer interaction without separation. However for this case, two shock waves corresponding to separation and reattachment shocks are seen and this is a clear indication that the separation region still exist.

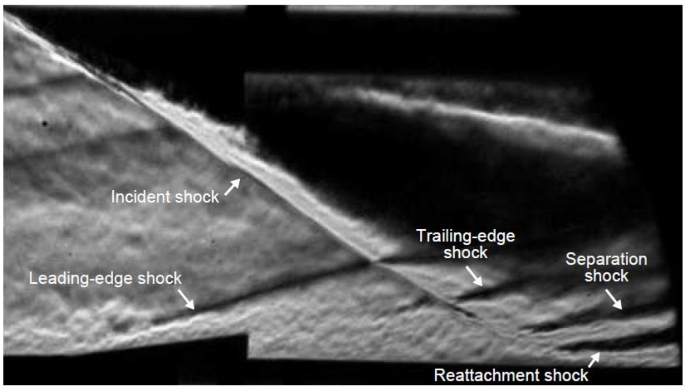

Figure 9: Instantaneous high-speed schlieren of interaction controlled by MVG

In Figure 10, from the oil-flow visualization image of the single MVG, the oil accumulation observed at the leading-edge of the model is caused by flow separation due to the incident angle. The flow is then observed to climb the surface of the model and subsequently moving towards the slant edges. As the flow moves down from the top surface of the model, counter-rotating vortices are formed as a result. The oil streaks at the middle of the model aligning with the apex of the MVG represents the primary vortices while the oil streaks emerging from the foot of the MVG is identified as the horseshoe vortices pair.

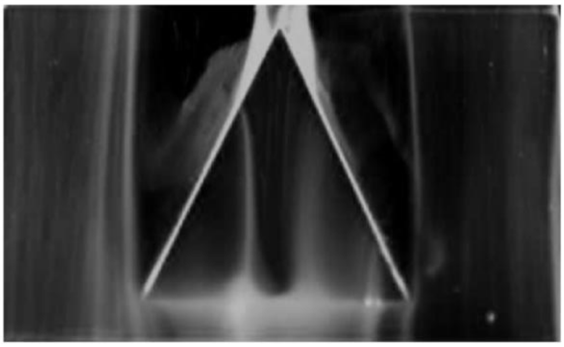

Figure 10: Oil-flow visualization of micro vortex generator. Note that flow is from bottom to top.

Another image shown in Figure 11 is the oil-flow on the surface of the interaction region where the oblique shock impinges on the boundary-layer. When the oblique shock impinges on the hypersonic boundary layer, a region of separated and reversed flow can be seen clearly using the oil-flow technique. Oil accumulation in the figure marks the start of the separation region forming the three-dimensional separation line while at a distance downstream, the reattachment region can observed from the termination of the oil streaks. Between the separation and reattachment line is the separation region, where reversed flow can be detected moving upstream from the reattachment line towards the separation line. Right after the reattachment line, the flow continues to move downstream, a sign of the boundary-layer reattachment.

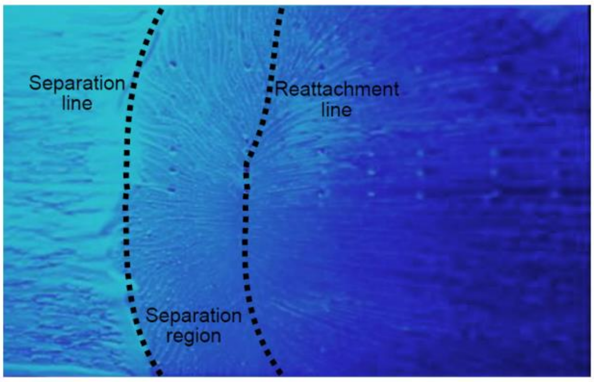

Figure 11: Oil-flow visualization of the interaction region without control (baseline)

The Pressure Sensitive Paints (PSP) resulted from the uncontrolled interaction (baseline) is shown in Figure 12. Note that the black dots represent the location of the pressure tappings utilised for in-situ calibration. The high-pressure region observed in between x = 2 to x = 6 is caused by the oblique shock-impingement which is the interaction region. The alternate streaks of high and low pressure inside the high pressure region are caused by the imperfect surface finish during the paint spraying process and not because of the three-dimensionality effect of the impinging shock wave. As an example between y = 3 to y = 5, a relatively low pressure area can be seen while the opposite is observed in the area between y = 2 to y = 5. However, since the pressure readings (shown later) are taken along the centreline (y = 0), these imperfections do not affect the results.

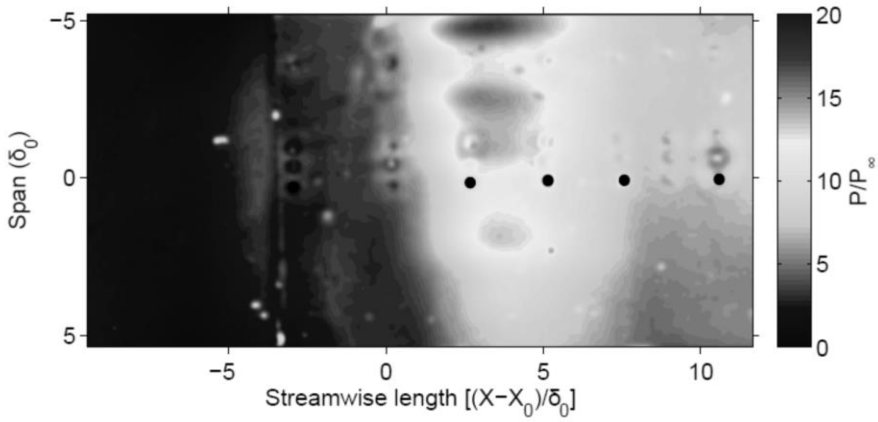

Figure 12: Pressure Sensitive Paints (PSP) image of uncontrolled interaction

Figure 13 shows the PSP image of the interaction region controlled by a single configuration MVG at the centreline. From the image it can be seen that no significant change of the interaction region can be spotted apart from the reduction of the intensity at the high-pressure streaks near the edge of the flat plate. However in order to quantitatively assess the improvement brought by the MVG, a pressure profile line was plotted on the centreline of the flat plate at $\delta_0 = 0$ as shown in Figure 14.

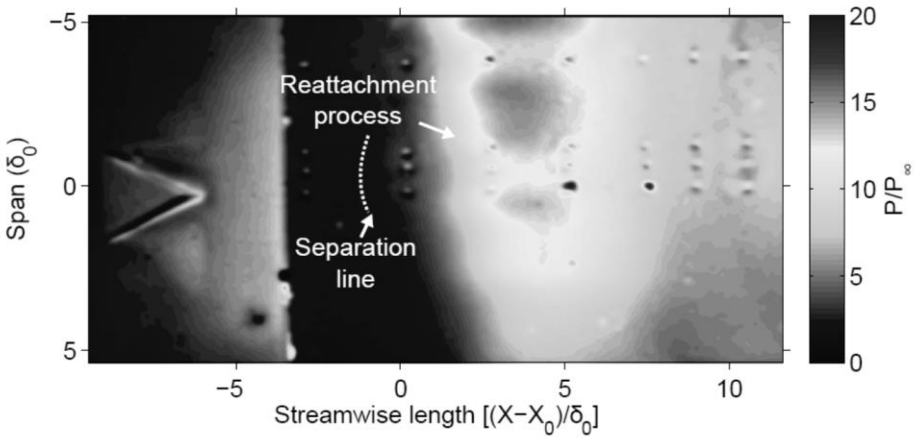

Figure 13: Pressure Sensitive Paints (PSP) image of controlled interaction by MVG

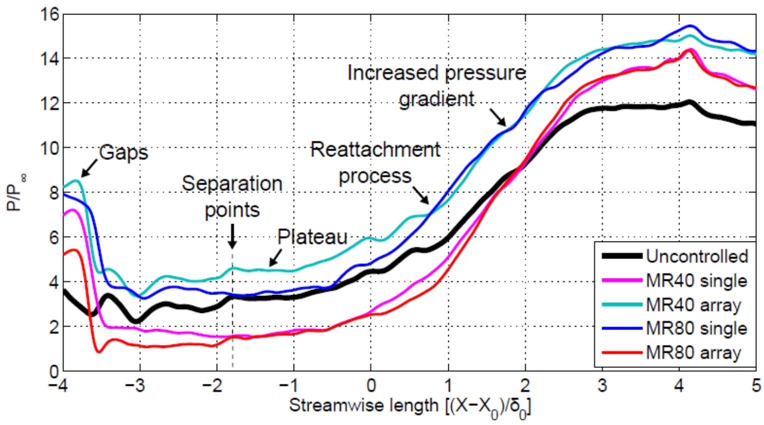

Figure 14: Surface pressure measurements using PSP along centreline for uncontrolled and controlled interaction

Based on Figure 14, for all MVG sizes, the pressure gradients after the reattachment process are significantly higher compared to the baseline case of uncontrolled interaction. This is a sign of the improvement of the separation caused by shock boundary layer interaction as also mentioned by Babinsky et al. [4]. Another indication is the peak pressures of all controlled case exceeded the peak pressure of the baseline, which is another sign of improvement.

4. Conclusion

The different experimental techniques and flow diagnostics used throughout this investigation proved to be beneficial in revealing the flow characteristics of the micro-vortex generator and also helped to understand more on the shock boundary layer interaction phenomenon. Oil-flow visualization and schlieren photography provided useful qualitative information on the flow physics especially in the interaction region, while employing PSP gave essential quantitative data in characterizing improvements brought by the micro-vortex generator in controlling SBLI. Investigations on hypersonic flow remain a big challenge especially for experimentalists, therefore employing the correct experimental technique and state-of-the-art flow diagnostics is definitely essential.

References

[1] Delery, J.M. 1985. Shock/wave/turbulent boundary layer interaction and its control. *Prog. Aerosp. Sci. 22*, 209–280.

[2] Dolling, D.S. 2001. Fifty years of shock-wave/boundary-layer interaction research: What next? *AIAA J.*, *39*, 1517–1532.

[3] McCormick, D.C. 1993. Shock/boundary layer interaction control with vortex generators and passive cavity. *AIAA J.*, *31*, 91–96.

[4] Babinsky, H., Li, Y., Pitt Ford C.W. 2009. Microramp control of supersonic oblique shock-wave/ boundary-layer interactions. *AIAA J.*, *47*, 668–675.

[5] Anderson, B.H.; Tinapple, J.; Surber, L. 2006. Optimal control of shock wave turbulent boundary layer interactions using micro-array actuation. In *Proceedings of the 3rd AIAA Flow Control Conference*, San Francisco, CA, USA, 5–8 June 2006; AIAA Paper 2006-3197.

[6] Blinde, P.L.; Humble, R.A.; van Oudheusden, B.W; Scarano, F. 2009. Effects of micro-ramps on a shock wave/turbulent boundary layer interaction. *Shock Waves*, *19*, 507–520.

[7] Saad, M.R., Zare-Behtash, H., Che-Idris, A., Kontis, K. 2012. Micro-Ramps for Hypersonic Flow Control. *Micromachines*, *3*, 364-378.

[8] Liu, T. & Sullivan, J.P. 2005. Pressure and Temperature Sensitive Paints. Springer-Verlag Berlin Heidelberg.